Int. J. Solids Structures, 1966, Vol. 2, pp. 319 to 335. Pergamon Press Ltd. Printed in Great Britain

CLAMPED CIRCULAR RIGID-PLASTIC PLATES UNDER CENTRAL BLAST LOADING

A. L. FLORENCE
Stanford Research Institute, Menlo Park, California

Abstract—A theoretical study is made of clamped circular plates of rigid-plastic material subjected to blast loading uniformly distributed over a central circular area. The dependence of the permanent central deflection on pressure, impulse and loaded area is obtained when the blast pulse is taken as a rectangular pulse.

1. INTRODUCTION

THE PROBLEM treated is the response of a clamped circular plate subjected to a suddenly applied pressure uniformly distributed over a central circular area. The pressure is assumed high enough or held on the plate long enough to produce moderately large plastic deformations. Although the governing equations are derived for a general pressure–time relationship they are solved only for the simplest case; that of a pressure held constant for a time and then suddenly released (a rectangular pulse). It is the variation of the permanent central deflection with pressure, impulse (area under the pressure–time curve) and the loaded area that constitutes the principal result. Because of interest in moderately large plastic deformations and in order to simplify the analysis the plate material is assumed to be rigid-perfectly plastic obeying the Tresca yield condition and the associated flow rule. Only the bending action of the plate is taken into account.

Past work on the dynamic response of a rigid-plastic circular plate concerns blast or impulsive loading uniformly distributed over the entire area. Wang and Hopkins [1] found the response of a clamped plate to an ideal impulse. A similar method of solution, the established continuity and jump conditions, and similar nomenclature are employed here. The responses of a simply-supported plate to an ideal impulse and a rectangular pulse were found by Wang [2] and by Hopkins and Prager [3] respectively. Recently the response of a clamped plate to a rectangular pulse was obtained [4].

The present problem is quite similar to that of [4] but, due to the loading covering only a central part of the plate (Fig. 1), two additional mechanisms of deformation can exist. An analogous situation exists for clamped beams [5].

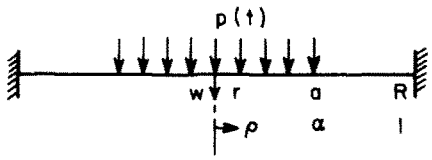

FIG. 1. Circular plate problem.

2. MECHANISMS OF DEFORMATION

A blast pulse may be idealized to the form shown in Fig. 2 with an instantaneous rise to the peak pressure p_m followed by a continuous monotonic decay. It is assumed that this form of pulse allows a steady progress through the various mechanisms of deformation that will be described.

FIG. 2. Idealized blast plate.

During deformation the plate is divided into annular regions in each of which exists a certain plastic regime defined by a vertex or side of the Tresca yield hexagon (Fig. 3) relating M and N, the radial and circumferential components of bending moment (positive moments cause tension on the underside of the plate). In this problem only the portion ABC is involved. Associated with these annular regions are velocity fields which must satisfy the flow rule, boundary conditions, and the appropriate continuity and discontinuity conditions [1].

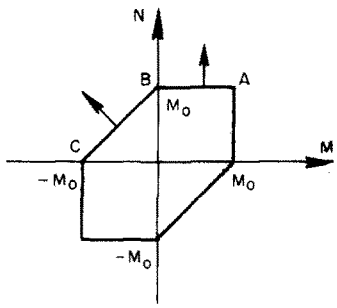

FIG. 3. Tresca yield hexagon.

From the equation of equilibrium, the static collapse pressure p_s, acting on a central circular area of radius $r = a$ of a plate of radius $r = R$, is found by assuming that in the circle $0 \leq r \leq r_s$, the plastic regime is AB, A being at the plate center and B at radius $r = r_s$, while in the outer annular region $r_s \leq r \leq R$ the plastic regime is BC, C being at the plate support $r = R$. The result may be expressed in the form [6]

$$p_s R^2 \alpha^2 (1 - 2\alpha/3\rho_s)/2M_0 = 1 \qquad 0 < \alpha \leq \rho_s \tag{1}$$

where ρ_s is the solution of

$$2\alpha\left(1 + \ln\frac{1}{\rho_s}\right)\Big/ 3\rho_s = 1 \tag{2}$$

and

$$p_s R^2 \rho_s^2 / 6M_0 = 1 \qquad \rho_s \leq \alpha \leq 1 \tag{3}$$

where now ρ_s is the solution of

$$\rho_s^2 \left(5 + 2 \ln \frac{1}{\rho_s}\right) = 3\alpha^2 \left(1 + 2 \ln \frac{1}{\alpha}\right) \tag{4}$$

In equations (1), (2), (3) and (4), $\rho_s = r_s/R$, $\alpha = a/R$ and M_0 is the fully plastic moment.

For values of the peak pressure in excess of the static collapse pressure the plate deforms initially in one of four mechanisms depending on the parameters $\lambda = p_m/p_s$ and $\alpha = a/R$.

(1) *Mechanism 3*

For large values of λ it is assumed that the initial mechanism of deformation consists of a central portion of radius $r_0(t)$ moving at a velocity $V(t)$, an outer annular portion $r_2(t) \leq r \leq R$ at rest, and an annular region between undergoing plastic deformation (Fig. 4). At $r = r_0(t)$ and $r = r_2(t)(r_0 < r_2)$ two plastic hinge circles exist and, for blast

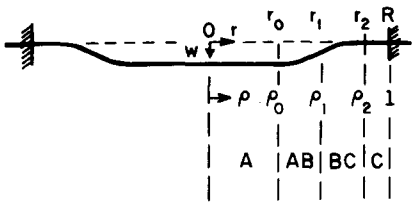

FIG. 4. Mechanism 3.

pulses of the kind shown in Fig. 2, the inner radius is assumed to decrease until the center is reached while the outer increases until the support is reached. At the radius $r = r_1(t)$ the plastic regime B exists and the rate of the radial component of curvature is discontinuous across this circle. The plastic regimes existing elsewhere are shown in Fig. 4. The velocity field meeting the above description, satisfying the flow rule, boundary conditions and the appropriate continuity and discontinuity conditions [1] is

$$w_t = \begin{cases} V & 0 \leq r \leq r_0(t) \\ V[1 - \sigma(r - r_0)/r_1] & r_0(t) \leq r \leq r_1(t) \\ V\sigma \ln \dfrac{r_2}{r} & r_1(t) \leq r \leq r_2(t) \\ 0 & r_2(t) \leq r \leq R \end{cases} \tag{5}$$

where

$$\frac{1}{\sigma} = \ln \frac{r_2}{r_1} + 1 - \frac{r_0}{r_1}.$$

In (5), w is the plate deflection and the subscript t denotes partial differentiation.

Deformation proceeds under another mechanism once one of the hinge circles reaches its terminal position. If the outer hinge circle reaches the support first the ensuing mechanism, called mechanism 2a, is described by the velocity field (5) with $r_2 = R$. If the inner hinge circle reaches the center first the ensuing mechanism, called mechanism 2b, is described by (5) with $r_0 = 0$. The final phase of deformation occurs after both traveling hinge circles have reached their terminal positions and the mechanism, called mechanism 1, is described by (5) with both $r_0 = 0$ and $r_2 = R$. This last mode is the same as that for static collapse [6].

(2) *Mechanism 2a*

This mechanism given by the velocity field (5) with $r_2 = R$ is an initial mechanism for certain ranges of α and λ. In fact, the range of α turns out to be $0{\cdot}56 \leq \alpha \leq 1$. The range of λ depends on α and is denoted by $\lambda_1 < \lambda \leq \lambda_2$ the numerical values for which are shown in Fig. 5.

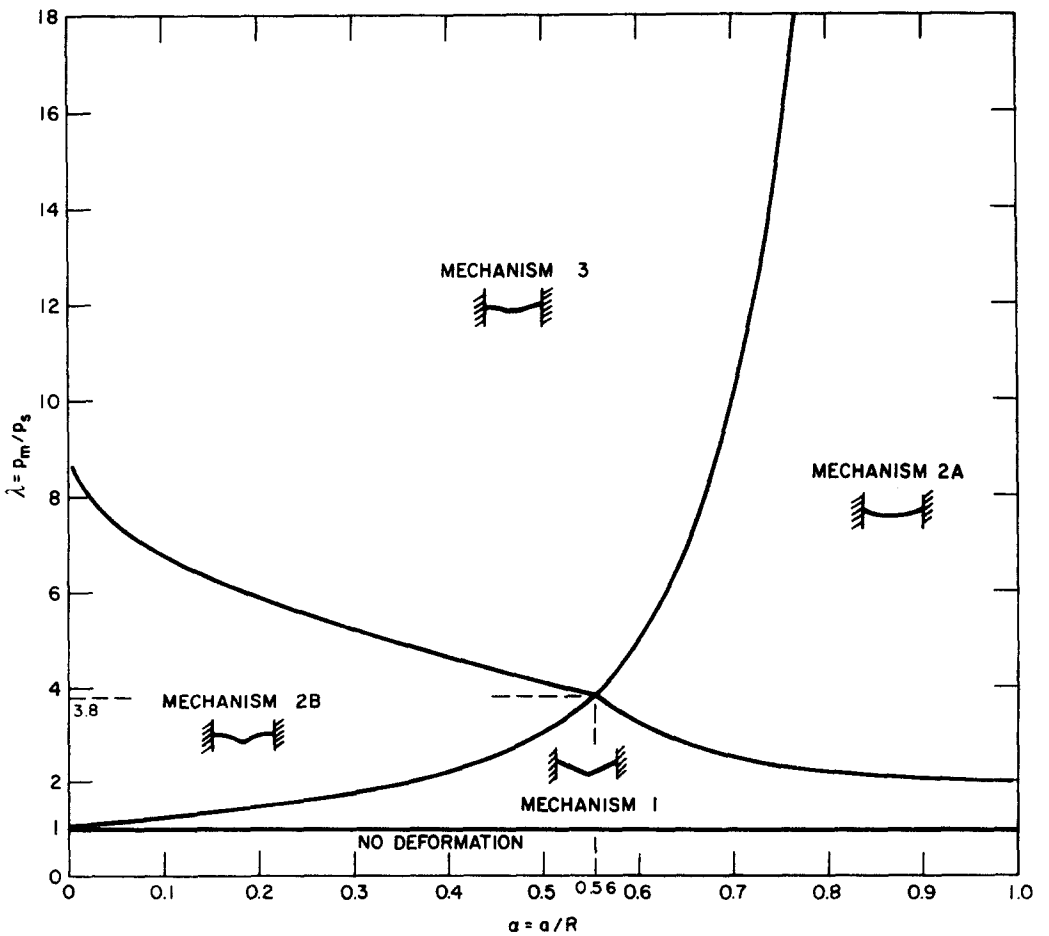

FIG. 5. Deformation mechanism diagram.

(3) *Mechanism 2b*

This mechanism given by (5) with $r_0 = 0$ is likewise an initial mechanism for certain ranges of α and λ. The range of α is $0 < \alpha \leq 0{\cdot}56$ while the range of λ depends on α and is again denoted by $\lambda_1 < \lambda \leq \lambda_2$ the numerical values for which are shown in Fig. 5.

(4) *Mechanism 1*

This mechanism, given by (5) with $r_0 = 0$ and $r_2 = R$, is an initial mechanism, and hence for blast pulses the only mechanism, for all α and for a certain range of λ depending on α. The range of λ denoted by $1 < \lambda \leq \lambda_1$ is obtainable from Fig. 5.

The way in which λ_1 and λ_2 are found is described once the governing equations are derived.

3. GOVERNING EQUATIONS

Independent of mechanisms the equation of motion is

$$N-(rM)_r = \int_0^r (p-mw_{tt})r\,\mathrm{d}r \tag{6}$$

where the subscripts r and t denote partial differentiation and m is the mass per unit area of plate. Differentiating the velocity (5) provides the acceleration to be substituted in (6) and the yield condition (Figs. 3 and 4) allows the circumferential component of bending moment N to be eliminated. Performing the integration in (6) and using the properties $M = M_0$ in $0 \leq r \leq r_0$, $M(r_1) = 0$, $M(r_2) = -M_0$ and $M_r(r_2) = 0$ leads to the following four equations governing mechanism 3.

$$V' = pR^2/12M_0 \tag{7}$$

$$\begin{aligned} &V'\eta(\xi_1-\xi_2+\eta)[\eta(6-8\eta+3\eta^2)+2(\xi_1-\xi_2)(3-3\eta+\eta^2)]-V\xi_1'\eta^2[\eta(1-\eta)(4-3\eta)\\ &\quad+(\xi_1-\xi_2)(6-8\eta+3\eta^2)]-V\xi_2'\eta^3(4-3\eta)-V\eta'\eta^2[\eta(4-3\eta)+2(\xi_1-\xi_2)(3-2\eta)]\\ &=\begin{cases}[(pR^2/6M_0\{3\alpha^2-2\alpha^3e^{\xi_1}-(1-\eta)^3e^{-2\xi_1}\}-1]e^{2\xi_1}(\xi_1-\xi_2+\eta)^2 & \alpha<\rho_1\\ [(pR^2/6M_0)e^{-2\xi_1}\eta(3-3\eta+\eta^2)-1]e^{2\xi_1}(\xi_1-\xi_2+\eta)^2 & \rho_1<\alpha\end{cases}\end{aligned} \tag{8}$$

$$\begin{aligned} &V'(\xi_1-\xi_2+\eta)[3e^{2(\xi_1-\xi_2)}-3-2(\xi_1-\xi_2)(3-3\eta+3\eta^2-\eta^3)]-V\xi_1'[3e^{2(\xi_1-\xi_2)}\\ &\quad-3-2(\xi_1-\xi_2)\{3-\eta^2(1-\eta)(3-2\eta)\}-2(\xi_1-\xi_2)^2(3-6\eta+6\eta^2-2\eta^3)]\\ &\quad-V\xi_2'[3e^{2(\xi_1-\xi_2)}\{\xi_1-\xi_2-(1-\eta)\}+(\xi_1-\xi_2)(3-6\eta+6\eta^2-2\eta^3)+3(1-\eta)]\\ &\quad-V\eta'[3e^{2(\xi_1-\xi_2)}-3-2(\xi_1-\xi_2)(3-3\eta^2+2\eta^3)-6(\xi_1-\xi_2)^2(1-\eta)^2]\\ &=\begin{cases}[\{(pR^2\alpha^2/2M_0)-1\}(\xi_1-\xi_2)-1]e^2\xi^1(\xi_1-\xi_2+\eta)^2 & \alpha<\rho_1\\ \left[(pR^2\alpha^2/4M_0)\left\{1-2\xi_2+2\ln\frac{1}{\alpha}-e^{-2\xi_2}/\alpha^2\right\}-(1+\xi_1-\xi_2)\right]e^{2\xi_1}(\xi_1-\xi_2+\eta)^2 & \\ \rho_1<\alpha\end{cases}\end{aligned} \tag{9}$$

$$V'(\xi_1-\xi_2+\eta)[3e^{2(\xi_1-\xi_2)}-3+2\eta(3-3\eta+\eta^2)]-V\xi_1'[3e^{2(\xi_1-\xi_2)}$$
$$-3-2(\xi_1-\xi_2)(3-6\eta+6\eta^2-2\eta^3)+2\eta^2(1-\eta)(3-2\eta)]V\xi_2'[3e^{2(\xi_1-\xi_2)}$$
$$\times\{2(\xi_1-\xi_2)-1+2\eta\}+3-6\eta+4\eta^2-2\eta^3]-V\eta'[3e^{2(\xi_1-\xi_2)}-3-6(\xi_1-\xi_2) \qquad (10)$$
$$(1-\eta)^2+2\eta^2(3-2\eta)]-V\xi_2'[3e^{2(\xi_1-\xi_2)}]$$
$$=[(pR^2\alpha^2/2M_0)-1]e^{2\xi_1}(\xi_1-\xi_2+\eta)^2 \qquad 0<\rho_2<1.$$

The new variables that have been introduced in the derivation of (8), (9) and (10) are defined by

$$\xi_1=\ln(1/\rho_1) \qquad \xi_2=\ln(1/\rho_2) \qquad \eta=1-\rho_0/\rho_1$$
$$\rho_0=r_0/R \qquad \rho_1=r_1/R \qquad \rho_2=r_2/R$$

Primes over the dependent variables V, ξ_1, ξ_2, and η denote differentiation with respect to the variable τ' where

$$\tau'=12M_0t/mR^2. \qquad (11)$$

The equations governing mechanisms 2a, 2b and 1 are readily obtained from (7), (8), (9) and (10) as outlined below.

(1) *Mechanism 2a*

The outer hinge circle is stationary at radius $r=r_2=R$ and the properties leading to the governing equations are $M=M_0$ in the region $0\le r\le r_0$, $M(r_1)=0$, and $M(R)=-M_0$. Consequently, the equations are (7), (8) and (9) with $\xi_2=\xi_2'=0$.

(2) *Mechanism 2b*

There is no inner hinge circle and the relevant properties are $M(r_1)=0$, $M(r_2)=-M_0$, and $M_r(r_2)=0$. Thus, the governing equations are (8), (9) and (10) with $\eta=1$ and $\eta'=0$.

(3) *Mechanism 1*

The outer hinge circle is stationary at radius $r=r_2=R$ and there is no inner hinge circle, leaving the two properties $M(r_1)=0$ and $M(R)=-M_0$, so the governing equations are (8) and (9) with $\xi_2=\xi_2'=0$, $\eta=1$, and $\eta'=0$.

Having now the equations governing motion in all four mechanisms it is possible to find the functions λ_1 and λ_2 shown in Fig. 5. It is assumed that the hinge circles and the circle $r=r_1$ have zero initial velocities so that $\xi_1'=\xi_2'=\eta'=0$ at $\tau'=0$. λ_1 is the upper bound of the values of λ for which mechanism 1 applies and the initial value of ξ_1, designated $\xi_1^{(0)}$, for each $\lambda=p_m/p_s$ or peak pressure p_m of this mechanism is obtained by solving the following two equations which are the appropriate special cases of (8) and (9):

$$V'(1+2\xi_1)=\begin{cases}[(p_mR^2/6M_0)\alpha^2(3-2\alpha e^{\xi_1})-1]e^{2\xi_1}(1+\xi_1) & \alpha<\rho_1\\ [(\rho_mR^2/6M_0)e^{-2\xi_1}-1]e^{2\xi_1}(1+\xi_1) & \rho_1<\alpha\end{cases} \qquad (12)$$

$$V'(3e^{2\xi_1}-3-4\xi_1) = \begin{cases} [(p_m R^2\alpha^2/2M_0)\xi_1-(1+\xi_1)]e^{2\xi_1}(1+\xi_1) & \alpha < \rho_1 \\ [(p_m R^2\alpha^2/4M_0)\left\{1+2\ln\frac{1}{\alpha}-e^{-2\xi_1}/\alpha^2\right\} & \\ -(1+\xi_1)]e^{2\xi_1}(1+\xi_1) & \rho_1 < \alpha. \end{cases} \tag{13}$$

By considering an increasing sequence of λ's the upper bound λ_1 is that value which causes an inflection point in the bending moment diagram for M either at the plate center or at the support. This means that the yield condition will be violated at these places for values of λ infinitesimally larger than λ_1. The conditions $M_{rr}(0, 0) = 0$ and $M_{rr}(R, 0) = 0$ are expressed by the equations

$$V' = p_m R^2/12M_0 \tag{14}$$

$$V'(3e^{2\xi_1}-1) = [(p_m R^2\alpha^2/2M_0)-1]e^{2\xi_1}(1+\xi_1) \tag{15}$$

and when $\lambda = \lambda_1$ either (14) or (15) is satisfied by the solutions $V'(0)$ and $\xi_1^{(0)}$ of (12) and (13). Computations show that whenever $0 \leq \alpha \leq 0{\cdot}56$, λ_1 is determined by the condition $M_{rr}(0, 0) = 0$ represented by (14), and whenever $0{\cdot}56 \leq \alpha \leq 1$, λ_1 is determined by the condition $M_{rr}(R, 0) = 0$ represented by (15). For further increases in λ_1 the former case indicates that the initial mechanism is 2b whereas for the latter it is 2a. The two portions of the λ_1 curve are shown in Fig. 5.

The values of λ_2 are found in a similar way. If the initial mechanism is 2a, the initial values $V'(0)$, $\xi_1^{(0)}$, and $\eta^{(0)}$ are obtained by solving for each $\lambda(\lambda > \lambda_1)$ or p_m equations (7), (8) and (9) with the special values $\xi_1' = \xi_2' = \eta' = 0$, and $\xi_2 = 0$. λ_2 is that value of λ which causes an inflection point in the bending moment diagram for M at the support. The condition $M_{rr}(R, 0) = 0$ is expressed by the equation

$$V'[3e^{2\xi_1}-3+2\eta(3-3\eta+\eta^2)] = [(p_m R^2\alpha^2/2M_0)-1]e^{2\xi_1}(1+\xi_1) \tag{16}$$

and when $\lambda = \lambda_2$, the initial values $V'(0)$, $\xi_1^{(0)}$ and $\eta^{(0)}$ satisfy (16). If the initial mechanism is 2b, the initial values $V'(0)$, $\xi_1^{(0)}$ and $\xi_2^{(0)}$ are obtained by solving for each $\lambda(\lambda > \lambda_1)$ or p_m equations (8), (9) and (10) with the special values $\xi_1' = \xi_2' = \eta' = 0$, and $\eta = 1$. λ_2 is that value of λ which causes an inflection point in the bending moment diagram for M at the plate center. The condition $M_{rr}(0, 0) = 0$ is expressed by the equation

$$V' = p_m R^2/12M_0 \tag{17}$$

and when $\lambda = \lambda_2$, the initial value $V'(0)$ satisfies (17). The two portions of the λ_2 curve are shown in Fig. 5.

4. SOLUTION FOR RECTANGULAR PULSE

Now follows an outline of the method of solution applicable to rectangular pulses with pressures high enough to cause initial deformation by mechanism 3. For the other initial mechanisms the method is similar and the details are simpler.

A solution is obtained if it is assumed that while the constant pressure is being applied the hinge circles and the circle of radius $r = r_1$ remain stationary. This phase of the motion, called phase 1a, involves the solution of equations (7), (8), (9) and (10) with the pressure p a constant $(\lambda > \lambda_2)$ and with the special values $\xi_1' = \xi_2' = \eta' = 0$. The solutions are denoted by $\xi_1^{(0)}$, $\xi_2^{(0)}$, and $\eta^{(0)}$. V' is given explicitly by (7). Corresponding to these

TABLE 1. INITIAL VALUES OF ρ_0, ρ_1, AND ρ_2

λ	$\alpha = 0{\cdot}438$				$\alpha = 0{\cdot}656$			
	$\rho_0^{(0)}$	$\rho_1^{(0)}$	$\rho_2^{(0)}$	Initial mechanism	$\rho_0^{(0)}$	$\rho_1^{(0)}$	$\rho_2^{(0)}$	Initial mechanism
1·05	0	0·492	1·0	1	0	0·635	1·0	1
1·1	0	0·487	1·0	1	0	0·636	1·0	1
1·2	0	0·480	1·0	1	0	0·637	1·0	1
1·5	0	0·460	1·0	1	0	0·639	1·0	1
2	0	0·438	1·0	1	0	0·643	1·0	1
2·5	0	0·423	0·987	2b	0	0·645	1·0	1
3	0	0·419	0·906	2b	0·039	0·648	1·0	2a
4	0	0·418	0·816	2b	0·143	0·649	1·0	2a
5	0	0·420	0·766	2b	0·200	0·648	1·0	2a
6					0·238	0·646	1·0	2a
7	0	0·424	0·709	2b	0·265	0·643	1·0	2a
8					0·292	0·643	0·983	3
10	0·186	0·428	0·662	3	0·337	0·646	0·947	3
15	0·239	0·431	0·619	3	0·402	0·649	0·892	3
50	0·335	0·436	0·536	3	0·523	0·654	0·784	3
100	0·366	0·437	0·507	3	0·564	0·655	0·747	3

values some initial values of the radii ρ_0, ρ_1, and ρ_2 are listed in Table 1 for two values of α. Note that as λ increases they tend to the radius α of the loading.

Let the pulse end at time $t = t_0$, or when $\tau' = \tau'_0$, and let the velocity and deflection of the plate center at this time be V_0 and δ_0. Then from equation (7) alone, successive integrations give

$$V_0 = I/m \tag{18}$$

and

$$\delta_0 = I^2/2mp \tag{19}$$

where $I = pt_0$ is the impulse applied per unit area.

When $t > t_0$, no pressure acts on the plate and, according to (7), the velocity of the plate center or rather the central region $0 \leq r \leq r_0$ is constant during this phase of motion, called phase 1b. It is evident from (8), (9) and (10) with $V' = p = 0$ that ξ_1, ξ_2, and η can no longer be treated as constants.

In equations (8), (9) and (10) set $V' = 0$, $V = V_0$ and, for convenience, introduce the nondimensional time variable τ defined by

$$t = mR^2\tau'/12M_0 = mR^2V_0\tau/12M_0. \tag{20}$$

The resulting equations, in indicial notation, may be written in the form

$$\xi_i' A_{ij} = B_j \qquad i, j = 1, 2, 3 \tag{21}$$

in which the derivatives are with respect to τ, and, for notational purposes only, $\xi_3 = \eta$.

The chosen numerical scheme for the solution of (21) commences by solving for the derivatives ξ_i' (equations (21) are linear in the derivatives) to give

$$\xi_i' = f_i(\xi_1, \xi_2, \xi_3) \qquad i = 1, 2, 3. \tag{22}$$

From (21) the variable τ can be eliminated resulting in the two equations

$$d\xi_1/d\xi_3 = g(\xi_1, \xi_2, \xi_3) \qquad \text{and} \qquad d\xi_2/d\xi_3 = h(\xi_1, \xi_2, \xi_3) \tag{23}$$

The initial values determined in phase 1a are $\xi_i^{(0)}$. From its initial value an incremental change is made in one of the variables here chosen to be ξ_3 so that its new value is $\xi_3^{(1)} = \xi_3^{(0)} + \Delta\xi_3$. Then, from (23), the corresponding new values of ξ_1 and ξ_2 are

$$\xi_1^{(1)} = \xi_1^{(0)} + g^{(0)}\Delta\xi_3$$

$$\xi_2^{(1)} = \xi_2^{(0)} + h^{(0)}\Delta\xi_3$$

where $g^{(0)} = g(\xi_1^{(0)}, \xi_2^{(0)}, \xi_3^{(0)})$ and $h^{(0)} = h(\xi_1^{(0)}, \xi_2^{(0)}, \xi_3^{(0)})$. With the values $\xi_i^{(1)}$ the new values $g^{(1)}$ and $h^{(1)}$ can be determined and hence $\xi_i^{(2)}$ can be calculated with the next increment $\Delta\xi_3 = \xi_3^{(2)} - \xi_3^{(1)}$. This procedure is continued until either $\xi_3 = \eta = 1$ or $\xi_2 = 0$. In the former case the deformation continues by mechanism 2b whereas in the latter case it continues by mechanism 2a. To find the value of τ_1 of τ at the end of phase 1b all the time increments are summed. The first of such increments is

$$\Delta\tau = \tau^{(1)} - \tau^{(0)} = (\xi_3^{(1)} - \xi_3^{(0)})/\xi_3'^{(0)}$$

in which $\xi_3'^{(0)} = f_3^{(0)}$ by (22).

Finally the deflection δ_1 of the plate center at the end of phase 1b is given by

$$\delta_1 - \delta_0 = V_0(t_1 - t_0) = I^2R^2(\tau_1 - \tau_0)/12mM_0 \tag{24}$$

in which δ_0 is determined by formula (19) and $\tau_0 = 12M_0/R^2p$.

As mentioned above the next phase of motion, called phase 1c, can take one of two forms depending on which hinge circle reaches its terminal position first. Only the case of the inner hinge circle of radius $r_0(t)$ reaching the center first will be described since the other case is covered by the description of phase 1b in the problem of Ref. [4], the only difference being in the initial values ξ_1 and η. (In [4], ξ plays the role of ξ_1.) Numerical calculations show that $r_0(t) = 0$ before $r_2(t) = R$ whenever $0 \leq \alpha \leq 0{\cdot}56$. The equations governing phase 1c for deformation by mechanism 2b are (8), (9) and (10) with the special values $p = 0$, $\eta' = 0$ and $\eta = 1$. For brevity, the indicial notation is used to express these equations in the form

$$\xi_i' C_{ij} = D_j \qquad i, j = 1, 2, 3. \tag{25}$$

In (25), derivatives are with respect to the time variable τ defined by (20) and, for notational purposes, $\xi_3 = \gamma = V/V_0$.

The numerical procedure is the same as that in phase 1b except that increments $\Delta\xi_2$ are used (instead of $\Delta\xi_3$) and the initial values are the final values of phase 1b. The procedure is halted at $\xi_2 = 0$ ($\rho_2 = 1$) when phase 1c ends. Let the central deflection and the time at the end of phase 1c be δ_2 and t_2 ($\tau = \tau_2$). Then

$$\tau_2 - \tau_1 = \sum_{n=1}^{N} \Delta\tau^{(n)}$$

where

$$\Delta\tau^{(n)} = (\xi_2^{(n)} - \xi_2^{(n-1)})/\xi_2'^{(n-1)}.$$

Also

$$\delta_2 - \delta_1 = \int_{t_1}^{t_2} V\,dt = \frac{I^2R^2}{12mM_0}\int_{\tau_1}^{\tau_2} \gamma(\tau)\,d\tau$$

which, by the numerical procedure adopted above, is replaced by the summation

$$\delta_2 - \delta_1 = \frac{I^2R^2}{12mM_0}\sum_{n=1}^{N} \gamma^{(n)}\Delta\tau^{(n)}. \tag{26}$$

In the final phase of motion, called phase 2, deformation is by mechanism 1 with the governing equations (8) and (9) having the special values $\xi_2' = \eta' = \xi_2 = p = 0$, and $\eta = 1$. So that the analysis of this phase conforms to those of [1] and [4], the variable τ is retained and the variable $\zeta = V/V_2$ is introduced where $V_2 = V(\tau_2)$. Then, the initial and final values of ζ are unity and zero. Also, the governing equations become

$$\zeta'(\xi_1+1)(2\xi_1+1) - \zeta\xi_1'\xi_1 = -(\xi_1+1)^2e^{2\xi_1}/\gamma_2 \tag{27}$$

$$\zeta'(\xi_1+1)(3e^{2\xi_1}-3-4\xi_1) - \zeta\xi_1'(3e^{2\xi_1}-3-6\xi_1-2\xi_1^2) = -(\xi_1+1)^3e^{2\xi_1}/\gamma_2 \tag{28}$$

in which differentiation is with respect to τ and $\gamma_2 = V_2/V_0$ (this is the value of γ at the end of phase 1c). Eliminating τ from (27) and (28) leads to a linear differential equation with the solution

$$\zeta = \left[\frac{\xi_1+1}{\xi_1(\tau_2)+1}\right]\exp\left[-\int_{\xi_1(\tau_2)}^{\xi_1}\frac{(1-\xi)\,d\xi}{4+7\xi+2\xi^2-3e^{2\xi}}\right]. \tag{29}$$

Motion ceases when $\zeta = 0$ and this occurs when $\xi_1 \approx 0{\cdot}478$ which is the solution of the equation

$$4+7\xi+2\xi^2-3e^{2\xi} = 0.$$

Let $\tau = \tau_3$ when motion ceases. Then

$$\tau_3 - \tau_2 = \int_{\xi_1(\tau_2)}^{\xi_1(\tau_3)}\frac{d\xi}{\xi'} = \gamma_2\int_{\xi_1(\tau_2)}^{\xi_1(\tau_3)}\frac{(3e^{2\xi}-4\xi^2-6\xi-3)\zeta\,d\xi}{e^{2\xi}(\xi+1)(4+7\xi+2\xi^2-3e^{2\xi})}. \tag{30}$$

Finally, let the central deflection when $\tau = \tau_3$ ($t = t_3$) be δ_3. Then

$$\delta_3 - \delta_2 = \frac{IR^2}{12M_0}\int_{\tau_2}^{\tau_3} V\,d\tau = \frac{I^2R^2}{12mM_0}\gamma_2^2\int_{\xi_1(\tau_2)}^{\xi_1(\tau_3)}\frac{(3e^{2\xi}-4\xi^2-6\xi-3)\zeta^2\,d\xi}{e^{2\xi}(\xi+1)(4+7\xi-2\xi^2-3e^{2\xi})}. \tag{31}$$

In Figs. 6 and 7 are shown the paths ABCD followed by the point (ξ_1, ξ_2, η) for values of α equal to 0·438 and 0·656 respectively,* both for $\lambda = 15$ which starts motion by

* These values of α were chosen to agree with values being used in an experimental program [7].

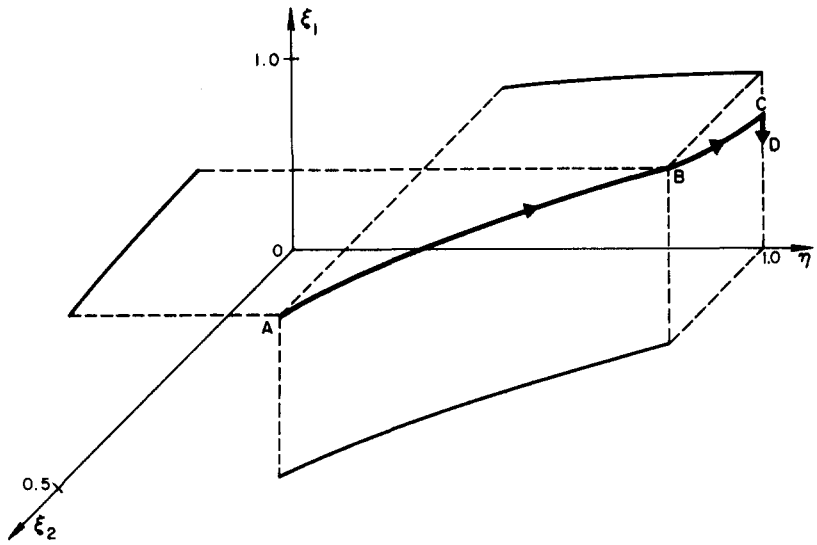

FIG. 6. Trajectory of (ξ_1, ξ_2, η) for $\alpha = 0{\cdot}438$ and $\lambda = 15$.

mechanism 3 (see Fig. 5 or Table 1). In the case of the smaller value of α Fig. 6 shows the trajectory starting at A and intersecting the plane $\eta = 1$ at B which corresponds to the value $\rho_0 = 0$. At this point of intersection the inner hinge circle has reached the center and the trajectory continues along BC in the plane $\eta = 1$ which corresponds to mechanism 2b. It next intersects the plane $\xi_2 = 0$ at C which corresponds to the value $\rho_2 = 0$. At this point of intersection the outer hinge circle has reached the support and

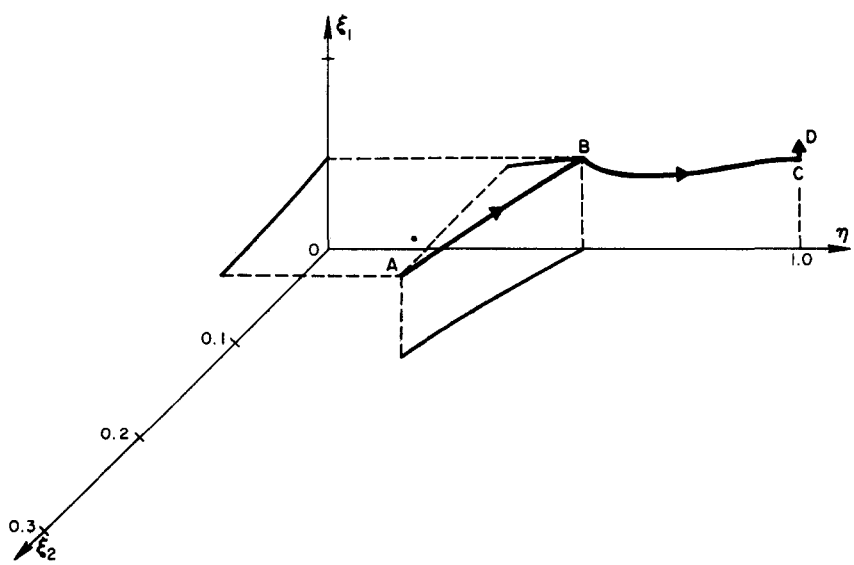

FIG. 7. Trajectory of (ξ_1, ξ_2, η) for $\alpha = 0{\cdot}656$ and $\lambda = 15$.

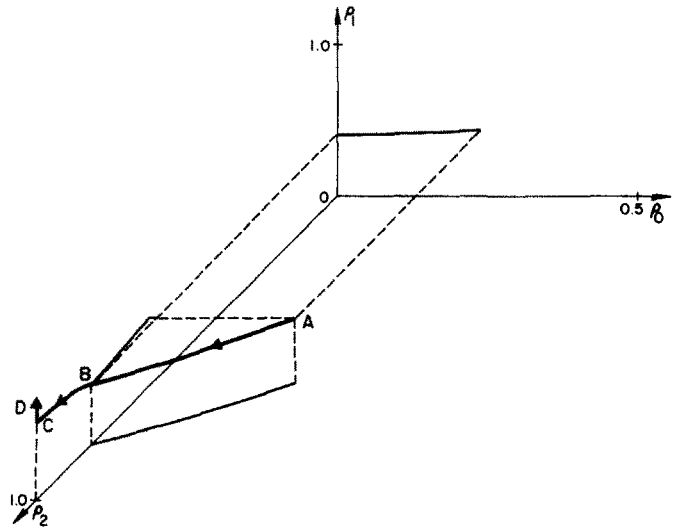

FIG. 8. Trajectory of (ρ_0, ρ_1, ρ_2) for $\alpha = 0{\cdot}438$ and $\lambda = 15$.

the trajectory continues along CD, the line of intersection of the planes $\xi_2 = 0$ and $\eta = 1$, corresponding to motion by mechanism 1. Figure 7 for $\alpha = 0{\cdot}656$ can be interpreted in a similar manner. Figures 8 and 9 show the trajectories ABCD in ρ_0, ρ_1, ρ_2 space.

Figures 10 and 11 show the variation of ρ_0, ρ_1, and ρ_2 with τ in all phases for values of α equal to 0·438 and 0·656 respectively, both for $\lambda = 15$. In each case the starting

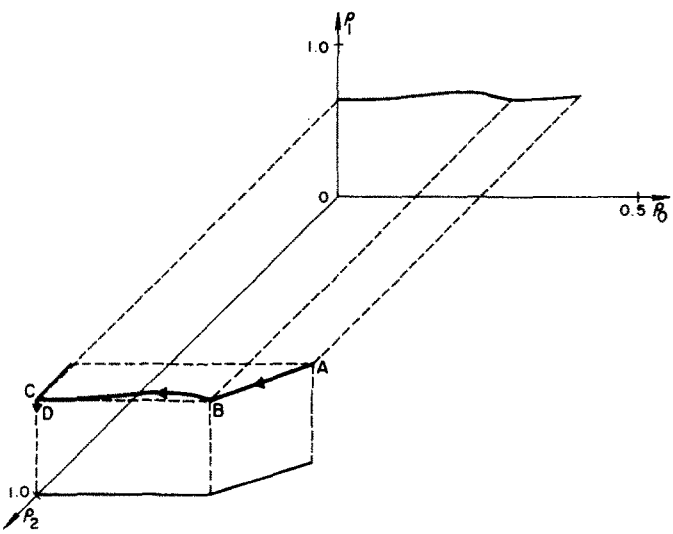

FIG. 9. Trajectory of (ρ_0, ρ_1, ρ_2) for $\alpha = 0{\cdot}656$ and $\lambda = 15$.

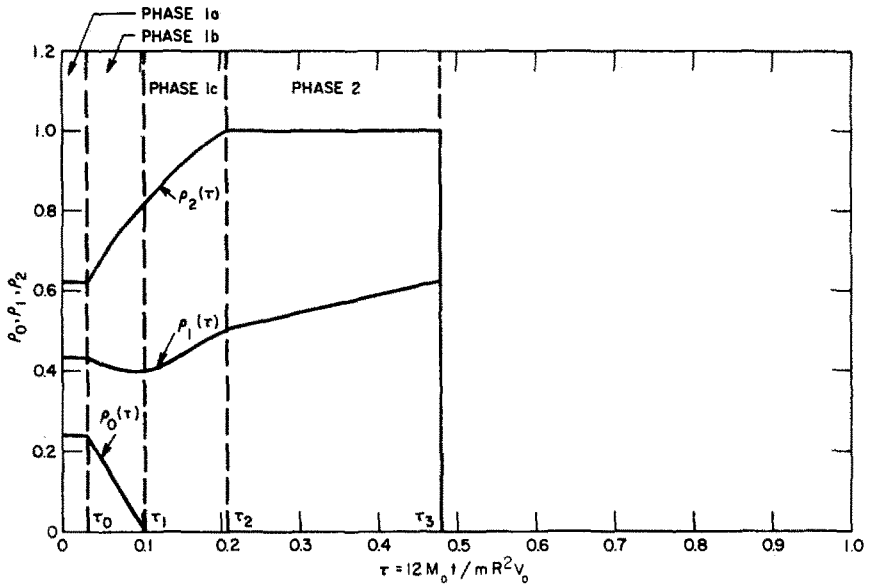

FIG. 10. Variation of ρ_0, ρ_1, and ρ_2 with τ for $\alpha = 0{\cdot}438$ and $\lambda = 15$.

values of ρ_1 are close to the loading radius α with ρ_0 and ρ_1 almost equally spaced on either side (see Table 1). The three radii are constant during phase 1a. The magnitudes of the average velocities of ρ_0 and ρ_2 in phase 1b are comparable. During phase 1b and, in Fig. 11, during phase 1c the values of ρ_0' are almost constant. During phase 2, ρ_0 is almost constant in Fig. 11 for $\alpha = 0{\cdot}656$ unlike that in Fig. 10 but like that in Fig. 12

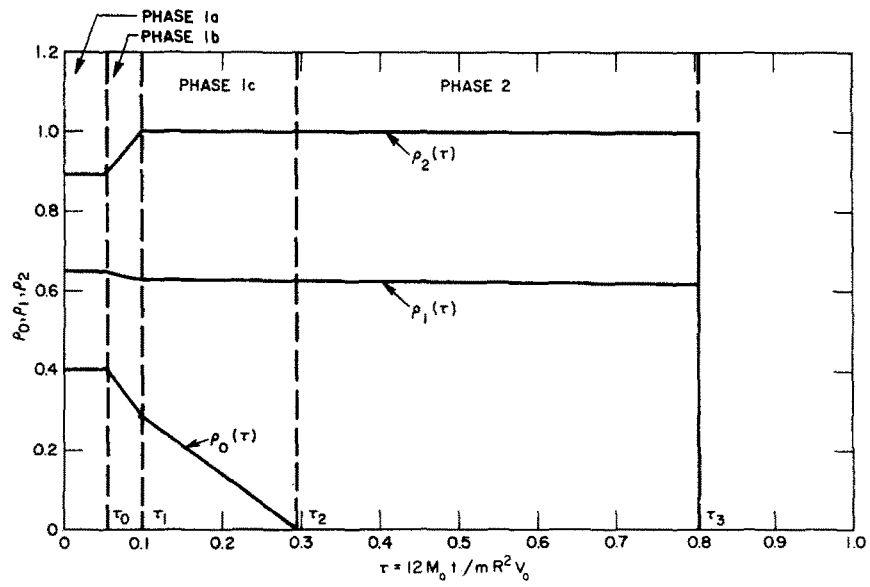

FIG. 11. Variation of ρ_0, ρ_1, and ρ_2 with τ for $\alpha = 0{\cdot}656$ and $\lambda = 15$.

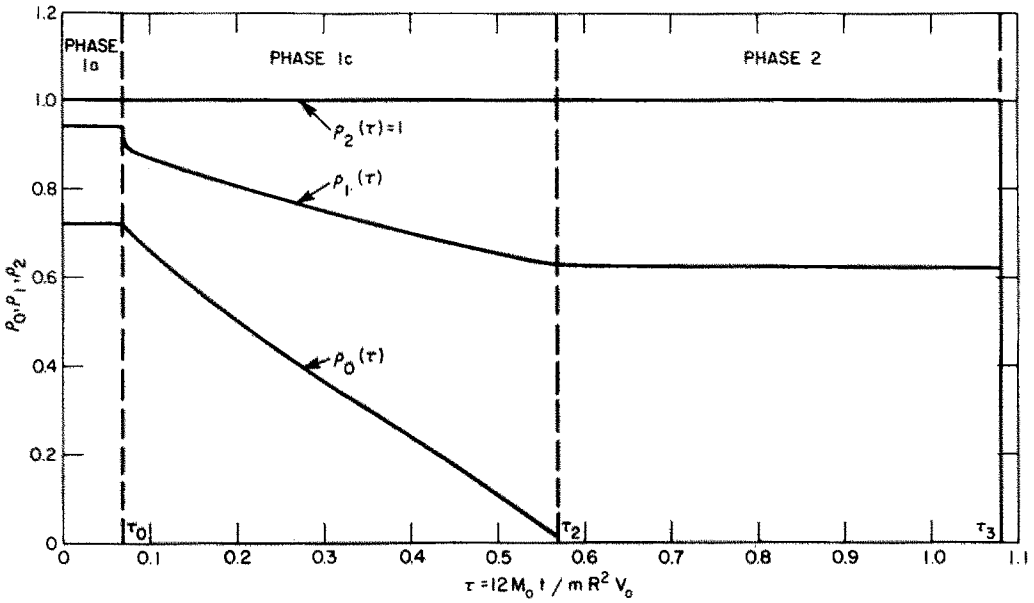

FIG. 12. Variation of ρ_0, ρ_1, and ρ_2 with τ for $\alpha = 1$ and $\lambda = 15{\cdot}7$.

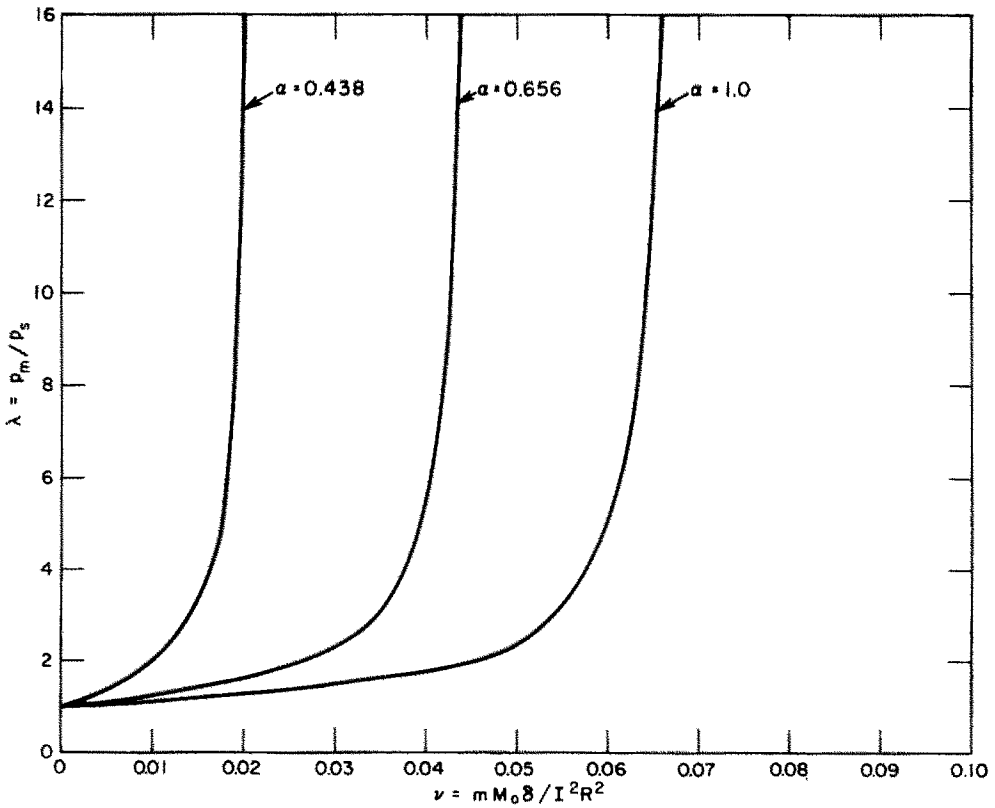

FIG. 13. Relationship among δ, λ and I.

which has been included to allow a comparison with the case $\alpha = 1$ ($\lambda = 15{\cdot}7$). The final value of τ, i.e. τ_3, increases with α which is to be expected because the work input increases with α.

5. RESULTS AND CONCLUSIONS

For three values of α Fig. 13 shows the relationship among the final central deflection δ, the impulse per unit area I, and the pressure p_m in the nondimensional form of λ versus $mM_0\delta/I^2R^2 = v$. The curve for $\alpha = 1{\cdot}0$ was obtained from the results in [4]. The three curves are alike. They start from the value $\lambda = 1$ where $\delta = 0$ and without curvature change tend monotonically toward vertical asymptotes. The location of these asymptotes have not been found for $\alpha = 0{\cdot}438$ and $\alpha = 0{\cdot}656$ but would be determined by considering the case of an ideal impulse ($\lambda = \infty$). However, judging by the case $\alpha = 1{\cdot}0$ for which the asymptote is known, the value of v when $\lambda = 100$ is sufficiently close. These values are 0·0212 and 0·0456 for α equal to 0·438 and 0·656 respectively. Figure 14 is another way of representing the same information and is essentially a pressure–impulse diagram.

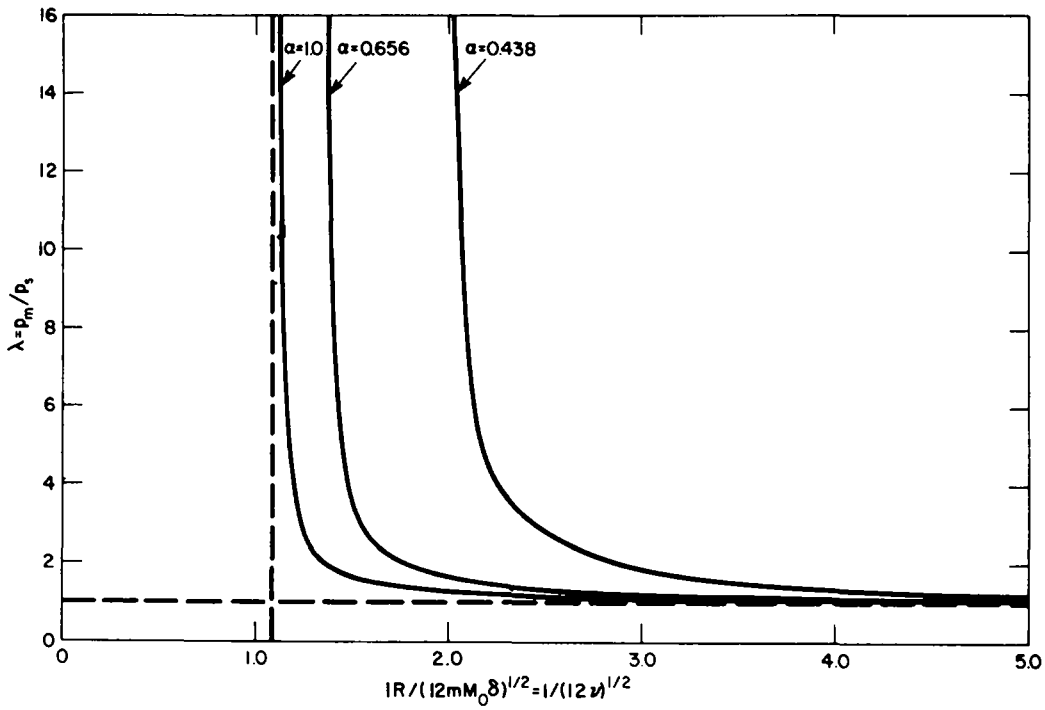

FIG. 14. Pressure–impulse diagram.

Figure 15 is a nondimensional plot relating the pressure to the loaded area considering as a parameter, v, which is proportional to the ratio δ/I^2. By treating both impulse and permanent central deflection as fixed quantities the curves show how the pressure must be increased as the loaded area decreases in order to maintain δ.

From Figs. 13, 14 and 15 the following conclusions can be drawn:

(1) For a given impulse, the central deflection δ increases monotonically with the pressure p_m becoming a maximum when the pressure is infinite, that is, when the given impulse is applied as an ideal impulse.

(2) Again for a given impulse, consideration of how δ increases with λ in Fig. 13 reveals that for $\alpha > 0{\cdot}438$ the central deflections are greater than 85 per cent of that due to an ideal impulse for pressures about seven times the corresponding static collapse pressure, that is, whenever $\lambda > 7$. Below this value of λ the decrease of λ with δ is quite pronounced.

(3) For a given central deflection δ, Fig. 14 shows that for $\lambda > 7$ ($\alpha > 0{\cdot}438$) the increase in impulse, over the ideal impulse, necessary to maintain the given deflection is less than 7 per cent. A large increase in impulse is required to maintain δ and λ decreases further, especially in the range $1 < \lambda < 3$.

(4) For a given permanent central deflection δ and a given impulse I Fig. 15 shows that the pressure required to maintain δ increases rapidly as the loaded area decreases, especially for $\alpha < 0{\cdot}6$ (for the values of ν shown).

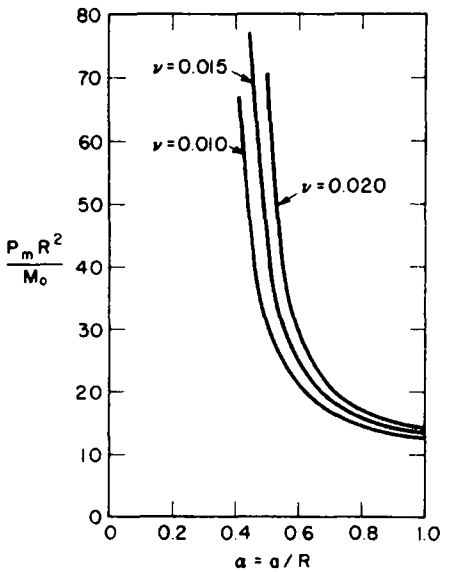

FIG. 15. Variation of pressure with loaded area.

Acknowledgements—The author is indebted to B. Bain for programming the B5500 computer and for providing Table 1 and Figs. 5–15.

This research was sponsored by the United States Air Force through the Air Force Weapons Laboratory under Contract AF 29(601)-6364.

REFERENCES

[1] A. J. WANG and H. G. HOPKINS, On the plastic deformation of built-in circular plates under impulsive loading. *J. Mech. Phys. Solids* **3**, 22 (1954).

[2] A. J. WANG, The permanent deflection of a plate under blast loading. *J. appl. Mech.* **22**, 375 (1955).

[3] H. G. HOPKINS and W. PRAGER, On the dynamics of plastic circular plates. *J. appl. Math. Phys.* **5**, 317 (1954).
[4] A. L. FLORENCE, "Clamped circular rigid-plastic plates under blast loading," presented at West Coast meeting of ASME, Los Angeles, 1965. *J. appl. Mech.* Paper No. 65-APMW-34.
[5] M. R. CONROY, The plastic deformation of built-in beams due to distributed dynamic loading. *J. appl. Mech.* **31**, 507 (1964).
[6] H. G. HOPKINS and W. PRAGER, The load carrying capacities of circular plates. *J. Mech. Phys. Solids* **2**, 1 (1953).
[7] A. L. FLORENCE, Development of long-duration explosive loading techniques and response of simple structures to pulse loads. Stanford Research Institute Final Report, Contract AF 29(601)-6364, AFWL TR-65-81, April 15, 1965.

(*Received* 12 *July* 1965)

Résumé—Etude théorique sur les plaques circulaires bridées en plastique rigide, soumises à une charge par souffle uniformément distribuée sur la surface centrale circulaire. La dépendance de la flexion centrale permanente sur la pression, l'impulsion et la surface chargée est obtenue au moment où l'impulsion du souffle est considérée comme impulsion rectangulaire.

Zusammenfassung—Eine theoretische Untersuchung von eingespannten kreisförmigen starr-plastischen Platten wurde ausgeführt, die einer gleichmässig verteilten Druckbelastung über einer zentralen kreisförmigen Fläche unterworfen sind. Die Abhängigkeit der anhaltenden zentralen Abweichung bei Druck, Impuls und belasteter Fläche wird erhalten wenn der Belastungsimpuls als ein rechtwinkliger Impuls angenommen wird.

Абстракт—Произведено теоретическое изучение зажимных круглых пластин из жесткопластигного материала, подвергнутых взрывной нагрузки однообразно распределённой по центральной круглой области. Зависимость постоянного центрального прогиба от давления, импульса и области загрузки получается тогда, когда импульс взрыва взят, как прямоугольный импуьлс.